Inhibition of receptor tyrosine kinases restores immunocompetence and improves immune-dependent chemotherapy against experimental leishmaniasis in mice

Jane E. Dalton, Asher Maroof, Benjamin M.J. Owens, Priyanka Narang, Katherine Johnson, Najmeeyah Brown, Lovisa Rosenquist, Lynette Beattie, Mark Coles, and Paul M. Kaye

Centre for Immunology and Infection, Hull York Medical School and Department of Biology, University of York, United Kingdom.

Receptor tyrosine kinases are involved in multiple cellular processes, and drugs that inhibit their action are used in the clinic to treat several types of cancer. However, the value of receptor tyrosine kinase inhibitors (RTKIs) for treating infectious disease has yet to be explored. Here, we have shown in mice that administration of the broad-spectrum RTKI sunitinib maleate (Sm) blocked the vascular remodeling and progressive splenomegaly associated with experimental visceral leishmaniasis. Furthermore, Sm treatment restored the integrity of the splenic microarchitecture. Although restoration of splenic architecture was accompanied by an increase in the frequency of IFN-γ^+CD4$^+$ T cells, Sm treatment alone was insufficient to cause a reduction in tissue parasite burden. However, preconditioning by short-term Sm treatment proved to be successful as an adjunct therapy, increasing the frequency of IFN-γ^+ and IFN-γ^+TNF$^+$CD4$^+$ T cells, enhancing NO production by splenic macrophages, and providing dose-sparing effects when combined with a first-line immune-dependent anti-leishmanial drug. We propose, therefore, that RTKIs may prove clinically useful as agents to restore immune competence before the administration of chemo- or immunotherapeutic drugs in the treatment of visceral leishmaniasis or other diseases involving lymphoid tissue remodeling, including cancer.

Introduction

Receptor tyrosine kinase inhibitors (RTKIs) are playing a growing role in the treatment of cancer, either as monotherapy or in combination with other anticancer drugs (1–3). Inhibition of changes in vasculature are well-documented outcomes of RTKI treatment (3–5), with the inhibitory effects of these drugs initially attributed to the blockade of VEGFRs and PDGFR (6). However, recent evidence suggests that the multitarget capabilities of RTKIs may underlie their beneficial effects in the treatment of chronic inflammation (3). Although drugs of this class have not been evaluated to date for efficacy in an infectious disease setting, their established pharmacokinetic and safety profiles and ready availability could lead to a significant and rapid impact on the treatment and control of major globally important diseases.

Visceral leishmaniasis (VL), caused by the protozoan parasites *Leishmania donovani* and *L. infantum*, is one of the most important of the neglected tropical diseases, with approximately 500,000 new cases and 70,000 deaths reported per annum (7, 8). Pentavalent antimonial drugs remain a first-line therapy for VL in most parts of the world, although increasing drug resistance now limits their use in India. Drug toxicity, increasing drug resistance, and a paucity of new drugs on the horizon (8) have focused attention on the need to develop new combined approaches to therapy, including therapeutic vaccination, and on the development of dose-sparing regimens (9, 10). The recognition that many antileishmanial drugs operate in synergy with host immune mechanisms (11) and some success with immunochemotherapy in humans (9, 12) have fueled further interest in defining molecular targets for immunotherapy, with CD40, CTLA4, OX40L, and IL-10R (13–16) all being validated in experimental models as candidates to boost T cell responses and enhance macrophage leishmanicidal activity.

Splenomegaly is a hallmark of both human and experimental VL. Studies in experimental models have been instrumental in deciphering the pathological changes that occur during splenomegaly (reviewed in ref. 17); these were conducted in the hope that a greater understanding of the processes involved might shed light on new therapeutic approaches. We have previously shown that progressive infection with *L. donovani* in mice is characterized by breakdown of splenic marginal zone architecture, with loss of marginal zone macrophages (MZMs) and repositioning of marginal metallophilic macrophages (MMMs) (17–20). Within the splenic white pulp, there is also disruption to both the follicular DC (FDC) network in B cell follicles (21) and the gp38$^+$ fibroblastic reticular cell (FRC) network that guides T cell and DC migration in the T cell zone (22). Similar alterations to splenic architecture are also observed in other infectious causes of splenomegaly, including experimental malaria (23, 24), trypanosomiasis (25), and following infection with LCMV (26–28); furthermore, although less well characterized, they are also a feature of human VL (29).

The importance of lymphoid tissue microanatomy, in particular of the stromal cell networks, is increasingly recognized as having a major influence on immune responsiveness (30–33). Thus, we and others have proposed that lymphoid tissue remodeling may be a common mechanism that underpins disease-associated immunosuppression (18, 22, 26, 28). Direct evidence in support of this concept has recently been obtained in mice infected with LCMV. This viral infection leads to transient splenomegaly and immu-

Conflict of interest: The authors have declared that no conflict of interest exists.
Citation for this article: *J Clin Invest.* 2010;120(4):1204–1216. doi:10.1172/JCI41281.

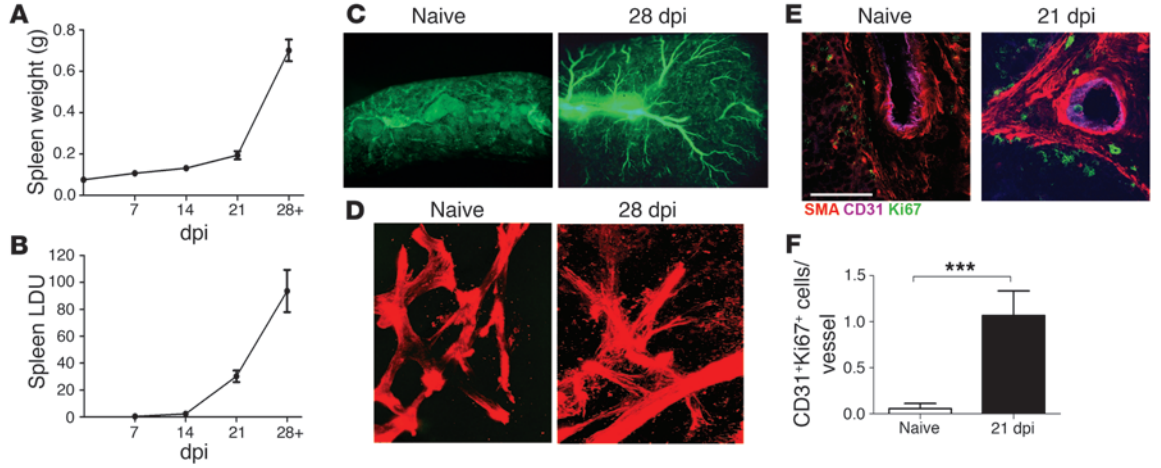

Figure 1

Vascular remodeling in *L. donovani*–infected spleens. (**A** and **B**) Spleen weights (**A**) and parasite burdens (**B**) measured during the course of infection. Data are mean ± SEM from 3 independent experiments (n = 8–10 per time point). (**C**) Splenic vasculature, visualized by FITC-dextran angiography, of naive versus infected (28 dpi) mice. Original magnification, ×12. (**D**) Whole mount staining of α-SMA$^+$ vasculature (red) in spleens from naive and 28-dpi mice. Images from Supplemental Videos 1 and 2 are shown. Original magnification, ×200. (**E**) Proliferation of vascular endothelial cells in infected mice, but not naive mice, analyzed by immunostaining of frozen spleen sections with CD31 (blue/purple), α-SMA (red), and the proliferation marker Ki67 (green). Scale bar: 100 μm. (**F**) Quantification of large-caliber vessels counted for CD31$^+$Ki67$^+$ cells. At least 4 vessels were counted per spleen section. Data are mean ± SEM of at least 2 independent experiments (n = 3 per time point). ***P = 0.0003.

nosuppression. However, as virus is cleared, normal lymphoid tissue architecture is restored, promoted by lymphoid tissue inducer (LTi) cells, and this process restores immune responses to third-party immunization (28).

Here, we provide the first direct evidence to our knowledge of vascular remodeling in the spleens of mice infected with *L. donovani* and show that treatment with the clinically validated RTKI sunitinib maleate (Sm) inhibited infection-associated splenomegaly. More striking, we show that Sm treatment induced a restoration of splenic microarchitecture, largely independent of the function of retinoid orphan–related receptor γ–dependent (RORγ-dependent) LTi cells, with a commensurate increase in immune competence. Furthermore, preconditioning with Sm was shown to be successful as a dose-sparing strategy for use with conventional antimonial drugs that are known to be immune dependent for their efficacy in vivo, with enhanced leishmanicidal activity during combined therapy attributable to increased local production of NO mediated by CD4$^+$ T cells producing IFN-γ and TNF. In addition to providing an approach for the treatment of VL in humans, our studies indicate what we believe to be a novel mode of action for broad spectrum RTKIs, namely the restoration of secondary lymphoid tissue architecture, which may also be of relevance to developing new strategies for the use of these drugs in cancer chemotherapy.

Results

Splenomegaly in experimental VL is accompanied by extensive vascular remodeling. A role for vascular remodeling in the development of splenomegaly associated with leishmaniasis was first suggested by electron microscopical studies of splenic architecture in dogs with progressive canine VL (34). We therefore first analyzed whether vascular changes occurred during the progression of *L. donovani* infection in mice at 14–28 days postinfection (dpi), when severe splenomegaly and increased tissue parasite burden became most evident (Figure 1, A and B). Injection of FITC-dextran followed by microangiography revealed substantial changes to the vascular network in the spleens of mice with chronic infection compared with spleens from uninfected control mice (Figure 1C). By whole-mount confocal microscopy, sprouting of α-SMA$^+$ vessels was clearly visible in spleens of chronically infected mice, but was not observed in the spleens of uninfected mice (Figure 1D and Supplemental Videos 1 and 2; supplemental material available online with this article; doi:10.1172/JCI41281DS1). To determine whether these vessels contained dividing vascular endothelial cells, we stained thin sections with the proliferation marker Ki67 (Figure 1E). Quantitative analysis confirmed an approximately 17-fold increase in the number of Ki67$^+$CD31$^+$ cells per cross-sectional vessel profile in the spleens of infected versus uninfected mice (P = 0.0003; Figure 1F). These data suggested that active endothelial cell proliferation was occurring in the spleens of mice with progressive VL.

The endothelial cell marker Meca32 identifies red and white pulp vasculature in the mouse spleen, including the marginal sinusoids (35). By confocal microscopy, expression of Meca32 was observed to increase over the course of infection, significantly so beginning at 14 dpi (P < 0.01; Figure 2A). CD31 expression, in contrast to that of Meca32, was restricted to the white pulp central arteriole and large-caliber vessels in the spleens of uninfected mice (Figure 2B). However, in infected mice, CD31 expression was progressively observed on what appeared to be newly emergent white pulp vessels (Figure 2B and Figure 3A). To determine whether these CD31$^+$ vessels represented new vascular growth, rather than merely vascular redistribution in the tissue, we used both thin sections (Figure 3A) and thick frozen sections (Supplemental Videos 3 and 4) to identify α-SMA, as a marker of perivascular mesenchymal cells. Whereas early after their appearance (14 dpi), white pulp CD31$^+$ vessels rarely stained for α-SMA, these vessels acquired α-SMA$^+$ mesenchymal cells over time. Quantitative analysis demonstrated that there was a significant increase in the frequency of CD31$^+$ vessels with accompanying α-SMA$^+$ mesenchymal cells (14 dpi, 32% ± 5% of all CD31$^+$ cells;

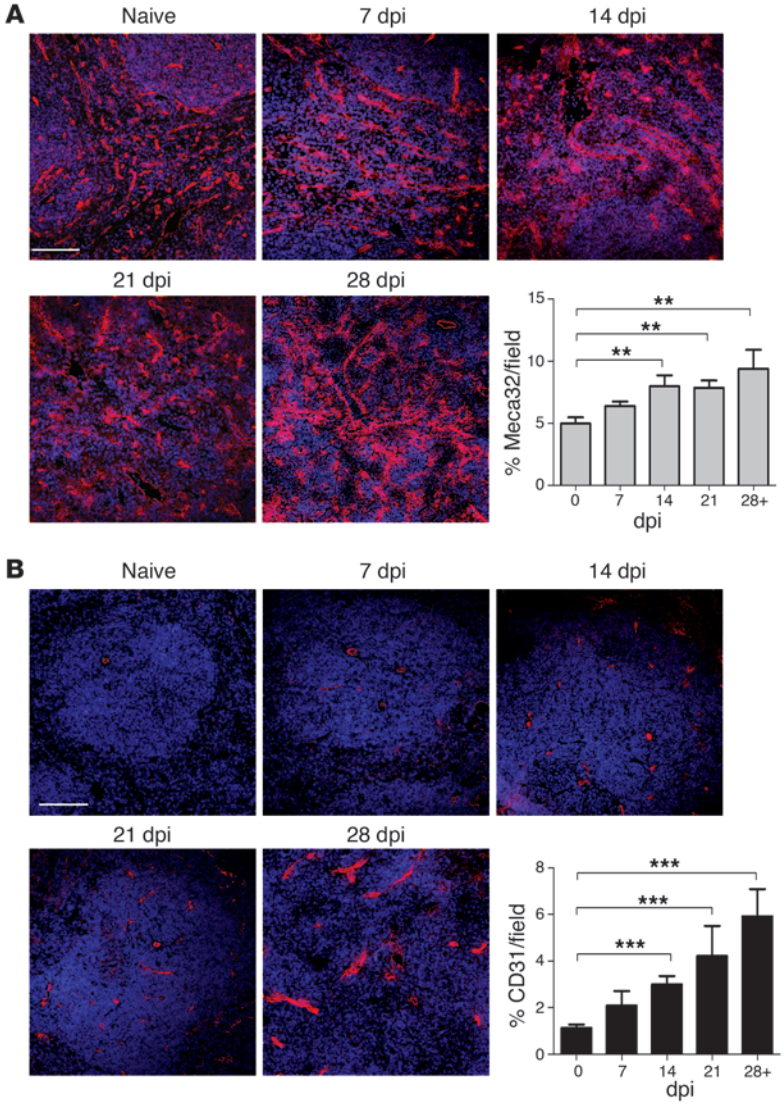

Figure 2
Increased expression of Meca32 and CD31 in *L. donovani*–infected spleens. (**A** and **B**) Expression of Meca32 (**A**) and CD31 (**B**) was determined (red) by immunostaining of frozen spleen sections from naive mice and mice at 7, 14, 21, and 28 dpi. Sections were counterstained with the nuclear dye DAPI (blue). Scale bars: 100 μm. Quantification of the area covered by Meca32$^+$ and CD31$^+$ endothelial cells in whole spleen was determined using computer-assisted morphometric analysis. A significant increase in the vascular area was observed in tissues beginning at 14 dpi compared with naive animals. Data are mean ± SEM of at least 3 independent experiments (n = 20 per time point). $^{**}P = 0.01$, $^{***}P < 0.0001$, ANOVA.

28 dpi, 90% ± 4%; Figure 3B). The marginal zone sinus also undergoes some disruption during experimental VL (19). However, we, as well as others working in murine models of malaria (24), noted that MAdCAM-1, the marker usually used to identify marginal sinus lining cells in the spleen, became expressed in a diffuse pattern across the white pulp after infection (Supplemental Figure 1), making it difficult to quantify changes in the marginal sinus with any degree of certainty. Nevertheless, our data collectively provide strong evidence that active vascular remodeling accompanies the development of progressive splenomegaly during VL.

Inhibition of splenomegaly and vascular remodeling by Sm. Sm is a broad-spectrum RTKI that targets VEGFR-1 and -2, CSF1-R, PDGFRα and β, cKIT receptor, and Flt-3 (36) and is approved for use in the treatment of renal cell cancer and imatinib-resistant or -intolerant GIST (37). As reversal of vascular remodeling is a suggested application of Sm (38), we used this drug to evaluate the effects of RTKIs on the development of splenomegaly and the outcome of infection. We adopted a standard protocol for testing anti-leishmanial drugs (16, 39), commencing 7 days of Sm therapy at 21 dpi. In untreated as well as vehicle-treated infected mice, spleen/body weight ratios increased 2- to 3-fold from 21 to 28 dpi (21 dpi, spleen weight 0.261 ± 0.03 g; 28 dpi treated with vehicle, 0.644 ± 0.06 g; $P = 0.008$; Figure 4A). In contrast, progressive splenomegaly did not occur in mice treated with Sm (spleen weight of 0.277 ± 0.06 g at 28 dpi). Oral administration of Sm inhibited progressive splenomegaly, but was not directly antiparasitic against amastigotes in macrophages in vitro (Supplemental Figure 2) and had minimal effects on total splenic parasite burden in vivo (Figure 4B and Table 1). In naive mice, Sm had no evident effect on splenic vasculature (Supplemental Figure 3), but treatment with Sm clearly reduced the extent of vessel branching in infected mice (Figure 4C). Quantitative analysis confirmed that Sm inhibited the progressive vascularization associated with splenomegaly, as measured by expression at 28 dpi of CD31 (vehicle, 8.9% ± 1.3% vascularization; Sm, 4.4% ± 0.5%; $P = 0.005$; Figure 4, D and F) and Meca32 (vehicle, 10.2% ± 0.8%; Sm, 7.1% ± 0.5%; $P = 0.004$; Figure 4, E and G). Thus, Sm could effectively inhibit ongoing vascular remodeling during experimental VL. The effect of Sm was short-lived, as expected from its lack of antiparasitic effect, and at 35 dpi, 7 days after cessation of treatment, spleen sizes were comparable in treated and untreated infected mice (0.59 ± 0.05 g and 0.57 ± 0.06 g, respectively).

Sm treatment reverses lymphoid tissue remodeling. We then determined whether blockade of RTKs affected splenic lymphoid tissue microarchitecture. As previously reported, splenomegaly in experimental VL is accompanied by disruption of MMMs in the inner marginal zone and loss of MZMs from the outer marginal zone, as well as by erosion of the FDC and FRC networks, with accompanying loss of T and B cell segregation and associated constitutive chemokine production (18, 21, 22). Disruption was already evident compared with naive mice at 21 dpi and was more extensive at 28 dpi in vehicle-treated infected mice. In contrast, infected mice treated with Sm showed almost complete reestablishment of T cell, B cell, and MMM positioning (Figure 5A). Sm treatment significantly restored the white pulp FRC network, as judged by gp38 staining (vehicle, 2.2% ± 0.5% of white pulp area; Sm, 5.1% ± 0.9%; $P = 0.016$; Figure 5, B and E). Likewise, Sm treatment restored the FDC network, as judged by either FDCM1 staining (vehicle, 5.8% ± 1.7%; Sm, 14.4% ± 3.5%; $P = 0.04$; Figure 5, C and F) or by CD35 staining

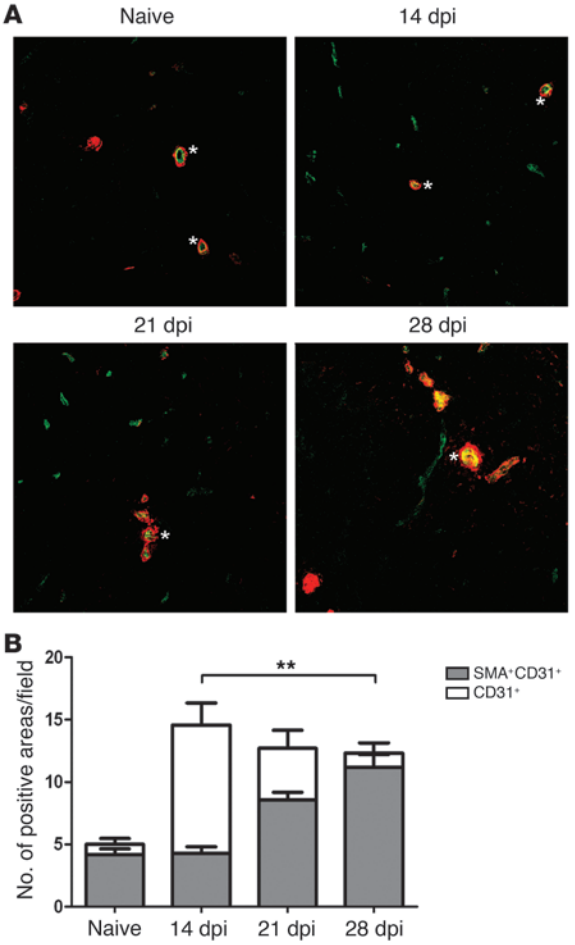

Figure 3
Vessel maturation during *L. donovani*–induced vascular remodeling. (**A**) Sections of frozen spleens taken during the course of *L. donovani* infection were stained with antibodies to CD31 and α-SMA. Fluorescent images highlight costaining of CD31$^+$ vessels (green) and α-SMA (red) on splenic white pulp vessels in naive mice and mice at 14, 21, and 28 dpi. Asterisks denote central arterioles. Note the increased expression of α-SMA on the CD31$^+$ vessels in the chronic stages of infection. Original magnification, ×200. (**B**) Quantification of CD31/SMA association during the course of *L. donovani* infection. The number of areas positive for CD31 was counted per field of view, and the number with intimately associated SMA staining was then determined. The combined data highlight the differences in the ratio of CD31$^+$ to SMA$^+$CD31$^+$ areas. At least 3 fields of view were counted per spleen section. Data are mean ± SEM of at least 2 independent experiments (n = 3 per time point). $^{**}P$ = 0.0012.

(data not shown). T cell zone CCL21 expression was also substantially restored by Sm treatment (Figure 5D). MZMs, which are lost by 21 dpi (19), did not reappear in drug-treated mice, as expected based on their slow repopulation kinetics (40). The total number of F4/80$^+$ splenic macrophages was not significantly affected by Sm treatment at 28 dpi (Sm, 3.14 ± 0.67 × 10^7 cells; vehicle, 5.9 ± 1.7 × 10^7 cells; P = NS). Sm treatment also had no effect on the frequency of splenic B cells, T cells, macrophages, or DCs or on total T cell number, but helped restore IgM^{hi} B cell localization in the marginal zone (Supplemental Figures 4 and 5). These data demonstrate the striking ability of an RTKI to restore lymphoid tissue architecture that had been otherwise remodeled during the course of a chronic infectious disease.

LTi cells are not required for lymphoid tissue reorganization after Sm treatment. Lineage$^-$CD3$^-$CD4$^+$CD45$^+$IL-7Rα$^+$ LTi cells have been reported to play an instrumental role in restoring stromal cell networks following recovery from LCMV infection (28), and the development of LTi cells has been shown to be critically dependent upon the transcription factor RORγ (41). Therefore, to determine whether there was also a role for LTi cells in the restoration of lymphoid tissue microenvironments that resulted from Sm treatment, we used the same approach as Scandella et al. and generated radiation chimeras using bone marrow cells derived from *Rorc*$^{-/-}$ mice. After 8 weeks, chimeras were analyzed for the presence of LTi cells. As expected (28), B6.*Rorc*$^{-/-}$→B6.CD45.1 chimeric mice had a greatly reduced (~90%) frequency of LTi cells compared with control B6→B6.CD45.1 chimeric mice, but normal levels of T cells, B cells, DCs, and macrophages (Figure 6A and Supplemental Figure 6). These chimeric mice were then infected with *L. donovani*; at 21 dpi, groups were treated with Sm or vehicle, and spleen histology was assessed 7 days later. In both control B6→B6.CD45.1 chimeras (LTi-sufficient) and B6.*Rorc*$^{-/-}$→B6.CD45.1 (LTi-deficient) infected mice, treatment with Sm resulted in marked improvement in T cell, B cell, and MMM positioning (Figure 6B) and a high degree of restoration to the FRC (Figure 6C) and FDC (Supplemental Figure 7) networks. These data suggest that, in contrast to that seen during natural resolution of splenic architecture following viral infection, LTi cells are not essential for restoration of splenic architecture following blockade of RTKs in this model.

Preconditioning with Sm partially restores immunocompetence in L. donovani–infected mice. Lymphoid tissue microanatomy is increasingly recognized as having a major influence on immune responsiveness (30–33), and we and others have proposed that lymphoid tissue remodeling may be a common mechanism that underpins disease-associated immunosuppression (18, 22, 26, 28). Such a causal link would imply that restoration of splenic architecture should improve immunocompetence in infected mice. IFN-γ, TNF, and IL-10 are key cytokines regulating host resistance and immune-dependent chemotherapy against *L. donovani* (39, 42), with data from human VL suggesting that IL-17A may also play a beneficial role (43). Therefore, we first sought to determine whether these cytokines could be detected directly ex vivo from mice infected with *L. donovani* and treated or not with Sm. At 7 days after cessation of Sm treatment, the frequency and number of CD4$^+$ T cells capable of secreting detectable amounts of IFN-γ without in vitro restimulation increased (Figure 7, A and B). In contrast, TNF-α– and IL-10–secreting cells were found at a much lower frequency and abundance, and there was no significant effect of Sm treatment (Figure 7, C–F). We could not detect IL-17a production in CD4$^+$ T cells by this method (data not shown). Furthermore, within the CD8$^+$ T cell population, we observed no impact of Sm treatment on the production of any of the cytokines examined (Figure 7, A–F). To further explore the production of IL-10 and IL-17a in the spleens of infected and treated mice, we performed real-time RT-PCR for *Il10* and *Il17a* mRNA. In comparison to mice treated with vehicle control, mice treated with Sm had decreased *Il10* mRNA accumulation and increased *Il17a* mRNA accumulation, suggesting that the production of these cytokines by cells other than T cells may occur following Sm treatment. Importantly, although

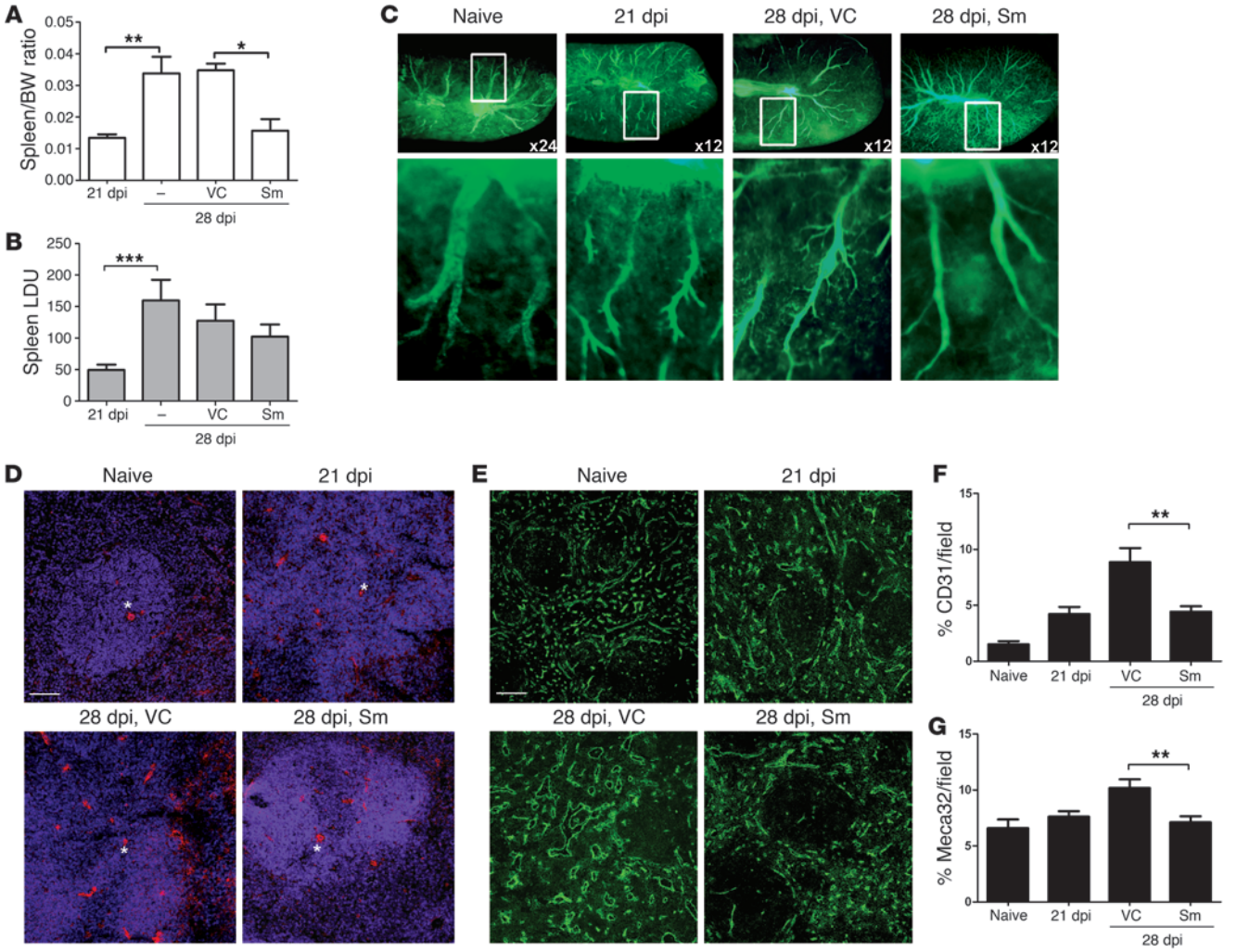

Figure 4

RTKI treatment inhibits pathogen-induced splenic vascular remodeling. (**A**) Spleen/body weight ratios in 21- and 28-dpi *L. donovani*–infected mice, measured before and after Sm treatment compared with vehicle control (VC) or no treatment. The significant increase in spleen weights and spleen/body weight ratios observed at 28 dpi compared with 21 dpi was inhibited by Sm treatment compared with vehicle control treatment. $^{*}P = 0.03$, $^{**}P = 0.008$. (**B**) Splenic parasite burdens were not altered by Sm treatment. $^{***}P = 0.006$. (**C**) Changes in splenic vasculature after Sm treatment, assessed by FITC-dextran angiography. Boxed regions are shown at higher magnification below, showing details of vascular branching. Original magnification, ×24 (naive, top); ×120 (naive, bottom); ×12 (infected, top); ×60 (infected, bottom). (**D**) Effect of Sm treatment on expression of CD31 (red) in *L. donovani*–infected spleens. Sections were counterstained with DAPI (blue). Scale bars: 100 μm. (**E**) Effect of Sm and vehicle control treatment on the expression of Meca32 (green) in *L. donovani*–infected compared with naive mouse spleens. Scale bars: 100 μm. (**F** and **G**) Area covered by $CD31^{+}$ (**F**) and $Meca32^{+}$ (**G**) endothelial cells in whole spleen following Sm treatment, determined using computer-assisted morphometric analysis. A significant decrease in the $CD31^{+}$ ($^{**}P = 0.005$) and $Meca32^{+}$ ($^{**}P = 0.004$) vascular areas was observed in tissues from Sm-treated mice compared with vehicle control–treated mice. Data are mean ± SEM of at least 3 independent experiments ($n = 5$ per time point).

these data indicate that the balance of effector and inhibitory responses and hence the overall level of immune competence of Sm-treated mice had improved, the magnitude of this response was clearly insufficient on its own to result in significant parasite killing (Figure 4B and Supplemental Figure 8).

Preconditioning with Sm provides a dose-sparing strategy for antimonial chemotherapy. Conventional chemotherapy for leishmaniasis involves the use of pentavalent antimonial drugs (sodium stibogluconate; Sb^{v}), and treatment of leishmaniasis with Sb^{v} represents a paradigm for cytokine-dependent chemotherapy (11, 44). IFN-γ and TNF have been shown in vitro, in experimental models, and (in the case of IFN-γ) in humans to synergize with antimonial drugs (45–47), and blockade of IL-10 is associated with improved chemotherapy (14). To establish proof-of-concept that treatment with a RTKI might, therefore, represent a route to develop dose-sparing regimens for conventional antileishmanial drugs, we treated *L. donovani*–infected mice with Sm at 21 dpi followed 7 days later with either an optimal (500 mg/kg) or a suboptimal (50 mg/kg) dose of Sb^{v} (14). Neither Sm treatment alone nor 50 mg/kg Sb^{v} alone induced significant leishmanicidal activity. In contrast, the sequential administration of these 2 drugs was highly effective, with parasite clearance after combined therapy achieving a level of

Table 1
Sm synergizes with low-dose antimonial chemotherapy

Treatment (dpi)		Spleen parasite burden (LDU)		Inhibition
21	28	28 dpi	35 dpi	(%)
VC	Saline	76 ± 10	64 ± 8	–
Sm	Saline	66 ± 9	86 ± 29	–
VC	Sb^v (50 mg/kg)		64 ± 10	0.2 ± 16
Sm	Sb^v (50 mg/kg)		26 ± 4[A]	70 ± 5[B]
VC	Sb^v (500 mg/kg)		1 ± 1	98 ± 1[B]
Sm	Sb^v (500 mg/kg)		6 ± 4	93 ± 4[B]

At 21 dpi with *L. donovani*, C57BL/6 mice were orally gavaged (daily for 7 days) with vehicle control (VC) or 35 mg/kg Sm. At 28 dpi, a cohort of mice was killed to determine parasite burden. The remaining mice received a single suboptimal (50 mg/kg) or optimal (500 mg/kg) dose of Sb^v i.p. or saline, and at 35 dpi, parasite burden and percent inhibition relative to appropriate saline controls were determined (11). Data (mean ± SEM) were pooled from 2 independent experiments (n = 10 per group). P values were calculated using ANOVA with post-test. [A]$P < 0.01$ versus vehicle plus Sb^v (50 mg/kg). [B]$P < 0.001$ versus relevant saline control.

effectiveness almost as high as that obtained with a 10-fold greater dose of Sb^v used as monotherapy (Table 1). To extend this observation, we next performed a dose ranging study to determine the extent to which Sm could synergize with lower doses of Sb^v (Figure 8A). From these data, we were able to calculate $ED_{50(spleen)}$ values for Sb^v when used as monotherapy (130 mg/kg) and when used in combination therapy with Sm as a preconditioning agent (26 mg/kg). Although we have focused here on the local effects of Sm on the control of splenic parasite burden, we also used data from this experiment to determine the impact on Sm preconditioning on the efficacy of Sb^v chemotherapy in the liver, another target organ of this infection. As in spleen, treatment with Sm alone had no impact on the outcome of hepatic infection (Supplemental Figure 8). However, Sm treatment reduced the calculated $ED_{50(liver)}$ for Sb^v from 226 mg/kg as monotherapy to 39 mg/kg in combined therapy, again representing a marked dose-sparing effect attributable to Sm preconditioning.

To gain further insight into the mechanism underlying the improved efficacy of this combined therapy approach, we analyzed intracellular cytokine production in $CD4^+$ T cells in greater detail in mice treated either with monotherapy or with Sm plus 50 mg/kg Sb^v as a combined therapy. In order to focus on antigen-specific cytokine responses and increase the likelihood of picking up polyfunctional responses, we restimulated $CD4^+$ T cells with *Leishmania* antigen-pulsed bone marrow–derived DCs (BMDCs) (48). High levels of intracellular IFN-γ and TNF were readily detectable in all groups of mice examined (Figure 8, B and D–F). Although we detected IL-10 at a low frequency, the frequency of $CD4^+$ T cells producing this cytokine did not vary among any of the treatment groups (Figure 8C). As with direct ex vivo staining, we also failed to detect any IL-17a after antigen restimulation of $CD3^+CD4^+$ T cell populations in these mice (Figure 8C). We then further analyzed the $CD4^+$ T cell response on the basis of whether cells produced IFN-γ and TNF singly or together (Figure 8, D–F). In keeping with earlier data (Figure 7), there was a trend in mice treated with Sm alone toward increased frequency of IFN-γ^+CD4^+ T cells, although, in contrast to results of direct ex vivo measurements, this was not significant with antigen restimulation. Similarly, mice treated with Sb^v alone also had a small but significant increase in the frequency of IFN-γ^+CD4^+ T cells. However, in mice treated with both Sm and Sb^v, the frequency of IFN-γ^+CD4^+ T cells was markedly increased compared with that in untreated infected mice or mice given either monotherapy (Figure 8D). The effects of these different drug regimens was also largely recapitulated within the IFN-γ^+TNF^+ coproducing $CD4^+$ T cell population (Figure 8E), but did not extend to single TNF-secreting $CD4^+$ T cells, where the frequency of response was unchanged by either monotherapy or combined therapy (Figure 8F). Finally, to determine whether these changes in known macrophage-activating cytokines translated into greater macrophage activation in situ, we examined the production of NO from splenic macrophages isolated from each treatment group (Figure 8G). These data showed a striking concordance with our cytokine analysis, with both Sm and Sb^v having a minimal impact on NO production when used as monotherapy, and a marked improvement in NO production as a result of combined therapy. Collectively, these data represent what we believe to be the first successful attempt at combination therapy for a parasitic infection using an RTKI and suggest a mode of action for this combined therapy that involves the enhancement of macrophage NO production driven by $CD4^+$ T cell–derived IFN-γ and TNF.

Discussion

RTKIs are potent drugs, known to have broad-spectrum effects but notable for their antiangiogenic properties. Although the pipeline for development of RTKIs has been fueled by diseases of the developed world, we demonstrate here that such drugs may also prove to be highly beneficial for VL, one of the most important of the neglected tropical diseases. We have demonstrated that the major pathological manifestations of experimental VL were inhibited with Sm, a licensed and widely available RTKI, that treatment with Sm enhanced endogenous $CD4^+$ T cell effector cell function, and that Sm provided dose-sparing synergistic effects in combination with conventional chemotherapy.

The spleen is a major target of infection in all forms of VL, and splenomegaly is a consistent clinical presentation. There have been few published studies, however, on the histopathology of human spleen during VL, and none that we are aware of have specifically examined the splenic microvasculature nor used immunochemistry to directly evaluate the positioning of specific lymphocyte, myeloid, or stromal cell populations. Nevertheless, we believe that from the available evidence, changes similar to those reported here in mice may occur in humans. First, in spite of clear anatomical differences in the microarchitecture of rodent and human spleen (33), H&E studies of human spleens taken from postmortem VL patients show white pulp atrophy, with loss of germinal centers, depletion of lymphocytes (presumptive T cells), follicular disruption, and extensive macrophage egress into the tissue (29, 49), all histopathologic changes that were also observed in experimental VL (17, 20) and in canine VL (50). Second, studies in canine VL have provided clear electron microscopical evidence for microvascular changes associated with progressive disease (34), data confirmed here by a variety of other approaches in experimental murine VL. Clearly, future immuno-histochemical analysis of the *L. donovani*–infected human spleen could provide further evidence to support the use of RTKIs for the treatment of this disease in humans.

These histopathologic changes in lymphoid tissue organization are likely to have a variety of sequelae that affect immune competence. In lymph nodes and spleen, elegant 2-photon imaging stud-

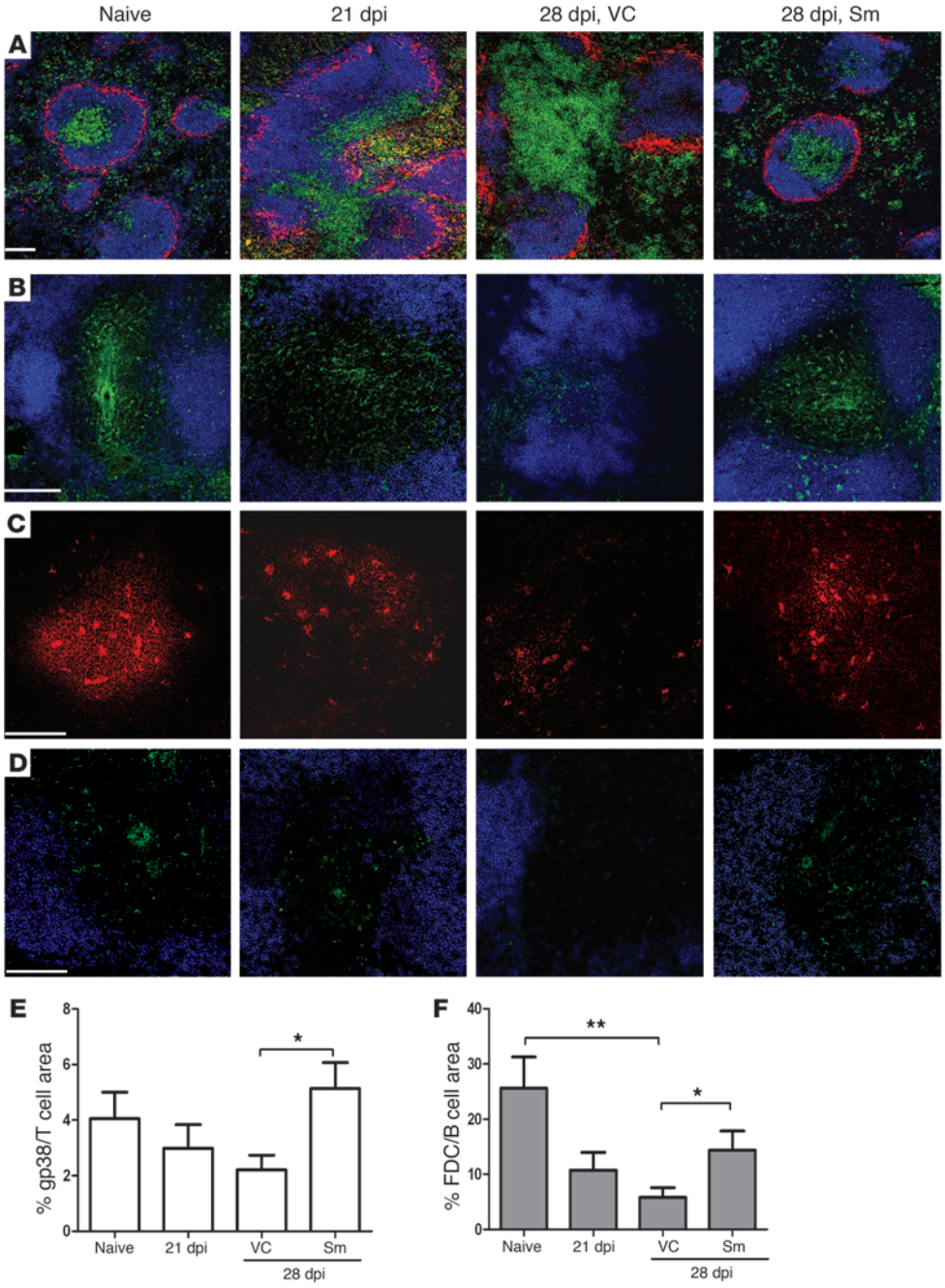

Figure 5
RTKI treatment restores pathogen-induced disruption of splenic architecture. (**A**) Immunofluorescent staining of frozen spleen sections (10 μm) before and after treatment with Sm showing localization of B cells (B220, blue), T cells (CD3, green), and MMM (MOMA-1, red). (**B**) Splenic T cell zones depicting FRC (gp38, green) and B cells (B220, blue). (**C**) Expression of FDC (FDCM1, red) in B cell follicles. (**D**) CCL21 (green) in T cell zones with B cells (B220, blue). Scale bars: 100 μm. (**E** and **F**) Area of gp38 staining in the T cell areas (**E**) and FDCM1 staining in B cell areas (**F**) after Sm treatment, determined using computer-assisted morphometric analysis. Data are mean ± SEM of at least 2 independent experiments (n = 3 per time point). $^{*}P < 0.05$, $^{**}P < 0.01$.

ies have recently revealed the importance of the FRC network, both as a guiding structure for T cell migration into, and as a modifier of T cell behavior within, the T cell zone (30, 51). This functional role for the FRC network, when taken in conjunction with our prior finding that the FRC network is remodeled during experimental VL (22), is entirely consistent with the observation that T cell migration into the periarteriolar lymphocytic sheath (PALS) is severely impaired in mice with VL (19). Mice with progressive VL also have defective traffic of DCs into the PALS, although this functional defect reflects IL-10–induced inhibition of CCR7 expression, rather than the defective production of CCL21 and CCL19 that occurs as a consequence of loss of the FRC network (22). Nevertheless, these 2 features of VL pathology allowed us to propose a model of immunosuppression based on spatial segregation of $CD4^+$ T cells and DCs (22, 52), and this model has subsequently been supported by observations made in other diseases (23, 26, 28). Given the evidence presented here that Sm treatment leads to both restoration of the FRC network and decreased *Il10* mRNA levels in the spleens of infected mice, it is reasonable to suggest enhancement of productive $CD4^+$ T cell–APC interactions as one of the mechanisms underlying the effectiveness of Sm preconditioning. Ongoing studies using intravital microscopy should determine whether this indeed does occur in situ.

From a functional standpoint, however, it is clear from our data that increased capacity to produce macrophage-activating cytokines is a major correlate of the effectiveness of combined chemotherapy

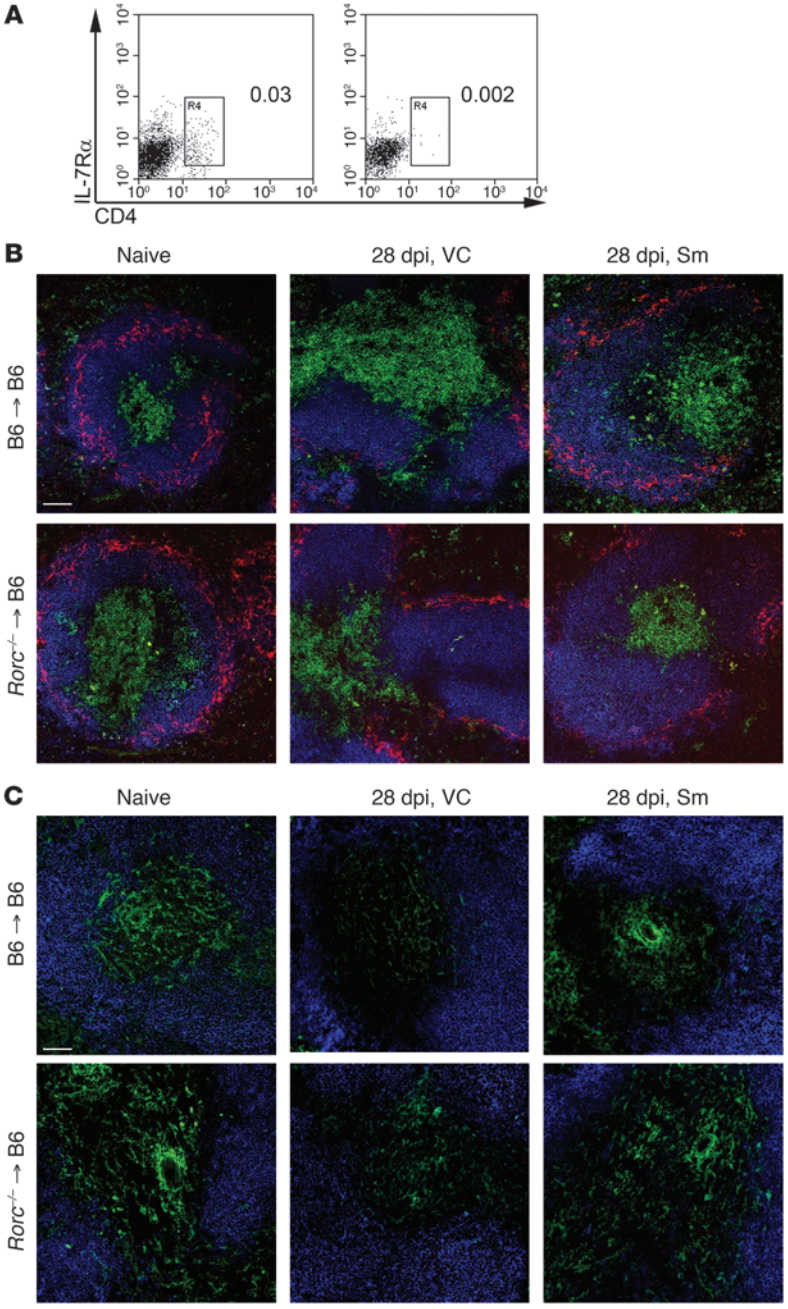

Figure 6
Restoration of splenic architecture after RTKI treatment is not dependent on LTi cells. (**A**) Flow cytometry analysis of LTi cells in the spleen of B6.*Rorc*$^{-/-}$→B6.CD45.1 chimeric mice (LTi insufficient; right) and B6.CD45.1→B6.CD45.1 chimeric mice (LTi sufficient; left). Plots are gated on CD11c^{-}B220^{-}CD3^{-}CD45^{+} cells; numbers denote percent LTi cells (IL-7Rα^{+}CD4^{+}) in spleen, as outlined by the boxed regions. Data are from 1 representative experiment (n = 3 per group). (**B**) Immunofluorescent staining of frozen spleen sections (10 μm) from naive and *L. donovani*–infected B6.*Rorc*$^{-/-}$→B6.CD45.1 and B6→B6.CD45.1 chimeras after treatment with Sm or vehicle control, highlighting localization of B cells (B220, blue), T cells (CD3, green), and MMM (CD169, red). (**C**) Splenic T cell zones depicting FRC (gp38, green) and B cells (B220, blue). Scale bar: 100 μm.

using Sm and Sb^{v}. Thus, whereas both drugs as monotherapy had relatively small effects on cytokine production, a minimal impact on endogenous NO production, and no leishmanicidal activity, the sequential administration of these drugs led to greater IFN-γ and TNF responses, substantially increased NO, and highly effective parasite clearance. Within this setting of sequential combined therapy, however, there are likely to be multiple layers of complexity. For example, the observed decrease in splenic IL-10 may, in addition to promoting increased APC function (22, 53), directly facilitate parasite killing within macrophages exposed to IFN-γ and TNF production (54). Similarly, alterations in IFN-γ induced by Sm preconditioning may also have effects on the local uptake and accumulation of Sb^{v} within macrophages (45), contributing to the reduction in ED_{50} we observed. Defining the relative contribution of these different pathways will require the future application of complex mouse models in which selective function can be ablated in a cell-specific and temporal manner.

Although we have identified multiple overlapping aspects of leishmaniasis pathology, dissection of any casual relationship(s) between the vascular remodeling and the lymphoid tissue remodeling associated with this disease also remains a substantial experimental challenge. For example, mononuclear phagocytes are known to play multiple roles in the pathogenesis of leishmaniasis: they act as host cells, regulators of immune function and as the final instrument of parasite killing (17); their cytokines are thought to contribute to lymphoid tissue remodeling (19, 22);

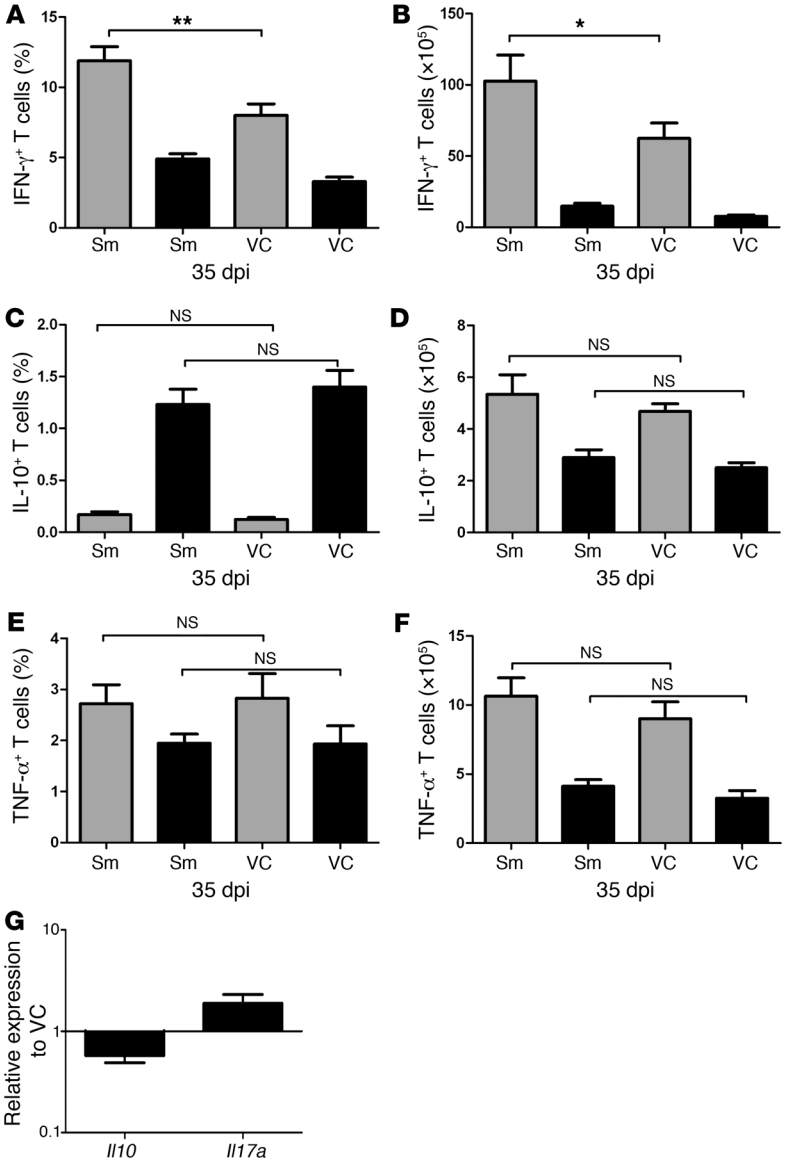

Figure 7
Treatment with Sm alters splenic cytokine responses. (**A**–**F**) At 35 dpi, 7 days after treatment with Sm or vehicle control, splenic $CD3^+CD4^+$ (gray) and $CD3^+CD8^+$ (black) T cells from *L. donovani*–infected mice were analyzed for intracellular IFN-γ (**A** and **B**), IL-10 (**C** and **D**), and TNF-α (**E** and **F**). Data are mean ± SEM and show both the frequency of T cells producing cytokines (**A**, **C**, and **E**) and the number of cytokine-producing cells per spleen (**B**, **D**, and **F**). $^*P < 0.05$, $^{**}P < 0.01$. (**G**) Spleen *Il10* and *Il17a* mRNA accumulation 7 days after treatment with Sm. Data are pooled from 2 independent experiments each ($n = 3$ per group) and expressed as fold difference relative to vehicle treatment.

and they are now recognized as important players in vascular remodeling in other systems (55–57). Thus, any intervention targeting macrophage function may have multiple downstream consequences. Similarly, vascular remodeling is intrinsic to the inflammatory process, with many inflammatory mediators having direct activity on vasculature and also the indirect ability to stimulate other cells to produce factors such as VEGF, PIGF, MCP-1, and TGFβ1 (58–60). Indeed, chronic inflammation and vascular remodeling are now regarded as codependent processes in many immune disorders (61–63). Nevertheless, future studies using more selective RTKIs may help unravel the multiple facets of this complex disease process.

LTi cells, in combination with lymphoid tissue organizing stromal cells, play a major role in lymphoid tissue organogenesis and immunity (64, 65); more recently, LTi cells have been implicated in the restoration of tissue architecture during the resolution of inflammation that follows LCMV infection (28). In spite of their importance, however, the study of LTi cells is hampered by the lack of precise phenotypic markers and of defined functional assays. The transcription factor RORγ is known to be essential for the development of LTi cells in all systems studied to date (41), and the use of chimeras generated using bone marrow from *Rorc*-deficient mice currently provides the only approach to evaluate the role of LTi cells in otherwise intact adult mice (28). Following the same procedures as described by Ludewig and colleagues, we generated chimeric mice that had significantly reduced numbers of $Lin^-CD3^-CD4^+CD45^+IL\text{-}7R\alpha^+$ LTi cells. These chimeras had normal numbers of other leukocyte subsets and developed levels of *Leishmania*-associated pathology similar to those of control chimeric mice, providing a means to evaluate whether LTi cells were involved in the restoration of architecture following Sm treatment. Surprisingly, following Sm treatment of B6.*Rorc*$^{-/-}$→B6.CD45.1 chimeric mice, tissue restoration occurred to a similar extent as seen in control B6→B6.CD45.1 mice. Although these data would appear to suggest a differential requirement for LTi cells in the restorative process that follows resolution of LCMV infection compared with that after Sm treatment during *L. donovani* infection, these data need to be interpreted with caution. First, as in all studies using chimeric mice, sufficient functional activity residing within a small number of residual recipient LTi cells cannot be excluded. Second, in the absence of an assay to reliably define LTi cell function in vitro or in vivo, it is not possible to exclude the possibility that in mice with chronic *Leishmania*-induced inflammation, there may be RORγ-independent development of cells that can functionally compensate for classical LTi cells. In this regard, our data are compatible with reports that tertiary lymphoid structures can develop in an LTi cell–independent manner, particularly under inflammatory conditions (66, 67).

With only a few notable exceptions, chemotherapy for VL has changed little in 50 years; in areas where drug resistance has yet to occur, it still involves parenteral administration of antimonial compounds (e.g., Pentostam and Glucantime). Amphotericin B, particularly in liposomal formulation (68), has become the drug of choice in developed countries and where antimony resistance is problematic, but issues of cost and toxicity remain (69). Oral miltefosine, recently shown to be effective in VL (70), has also more recently been shown to be compatible for use in

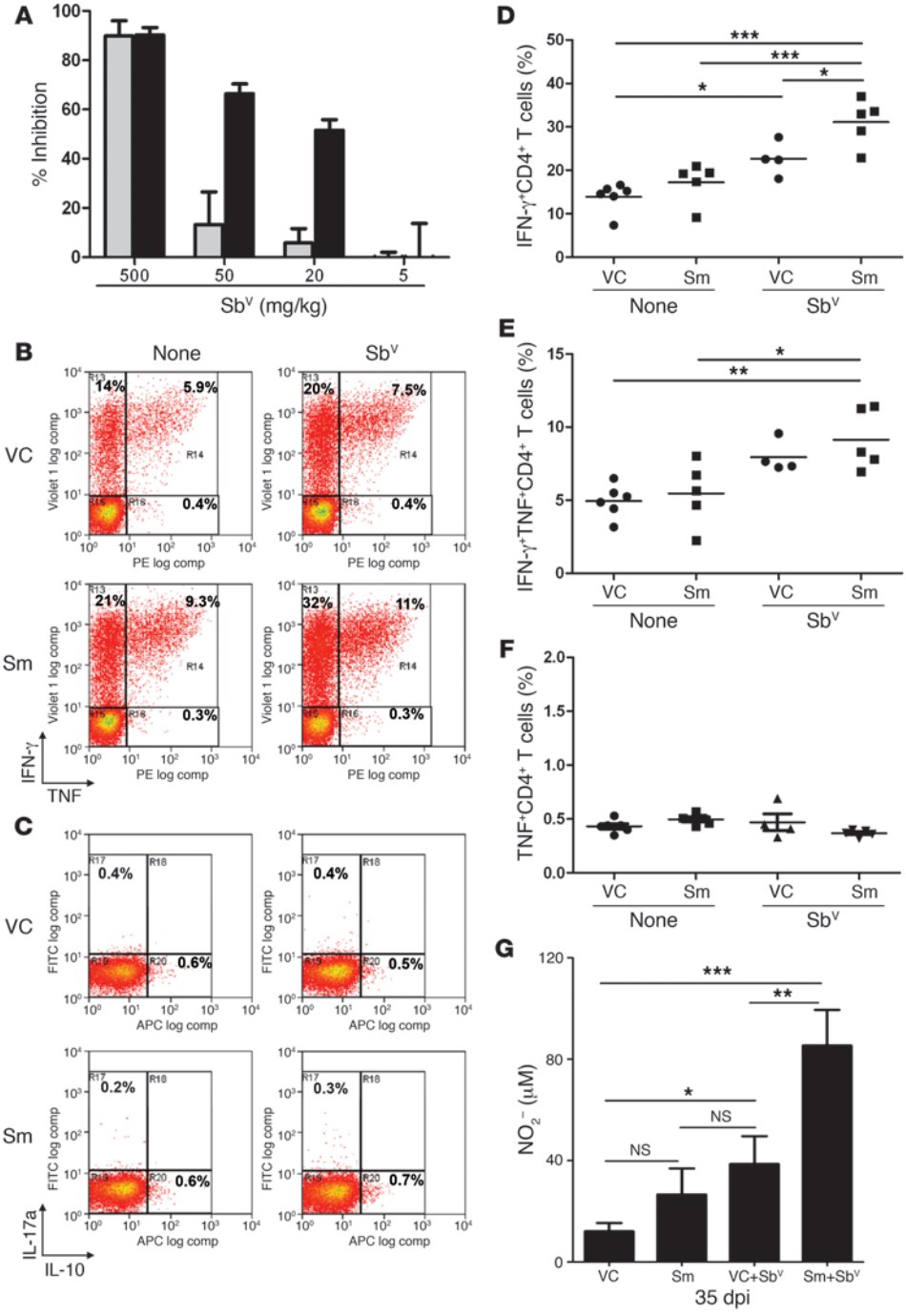

Figure 8
Highly effective sequential therapy with Sm and Sb^V enhances CD4$^+$ T cell cytokine responses and splenic NO production. (**A**) Groups of *L. donovani*–infected mice were treated from 21 to 28 dpi with Sm (black) or vehicle (gray) and then given a single i.p. injection of Sb^V at the doses indicated. Percent inhibition in spleen parasite burden (determined as LDU) was calculated relative to that of untreated infected mice (108 ± 15 LDU). Data are mean ± SEM (n = 6 per group). (**B** and **C**) Splenic CD3$^+$CD4$^+$ from Sm- and vehicle control–treated mice with or without additional Sb^V therapy were restimulated with *L. donovani*–infected BMDCs and analyzed by multicolor flow cytometry for intracellular IFN-γ and TNF (**B**) as well as IL-10 and IL-17a (**C**). Dot plots show representative mice from data pooled in **D**–**F**. (**D**–**F**) Frequency of CD3$^+$CD4$^+$ T cells from the indicated treatment groups that produced IFN-γ alone (**D**), IFN-γ and TNF (**E**), and TNF alone (**F**). (**G**) NO production by adherent splenocytes from infected mice treated as indicated. Data (mean ± SEM) are from 1 experiment (n = 6 per group). $^*P < 0.05$, $^{**}P < 0.01$, $^{***}P < 0.001$.

combination therapy with Amphotericin B (71). Of note, it has been long recognized from studies in experimental VL that the efficacy of the antimonial drugs is exquisitely dependent upon host immune function, being modulated by a number of key T cell–derived cytokines (11, 14, 44). Although amphotericin B is less immune dependent in its mode of action in mice (11), clinical experience in the treatment of VL in HIV-infected patients, using this drug (72) as well as miltefosine (73), suggest that in humans, all antileishmanial drugs in current use probably have some degree of dependency on host immune effector mechanisms, particularly when measured in terms of the frequency of relapse. Hence, we believe that the restoration of immune competence described here could prove beneficial in combination with a variety of established therapeutic modalities.

In conclusion, concerns about severe side effects from drug toxicity in the treatment of leishmaniasis, such as nephrotoxicity (74), pancreatitis (75), and hepatotoxicity (76, 77) along with the development of drug resistance (78), have led to a need for the development of combined therapies for the leishmaniases, and notably for VL and drug-resistant cutaneous leishmaniasis. Our data suggest that a short-duration preconditioning regimen using broad-spectrum RTKIs, if proven safe in patients with active leishmaniasis,

may help meet this major unmet clinical need. Furthermore, given that some conventional cancer drugs also depend upon immune responses for their efficacy (79), and with mounting evidence for the immune dependence of chemotherapy against other globally important infections such as malaria (80), the ability of RTKIs to restore the damage to lymphoid tissue architecture induced by chronic inflammation may be of value in other diseases in which splenomegaly and/or lymphoid tissue remodeling are apparent.

Methods

Experimental infection and treatment. C57BL/6 CD45.1 and CD45.2 mice were obtained from Charles River UK, housed under specific pathogen–free conditions, and used at 6–10 weeks of age. *Rorc*$^{-/-}$ mice, originally obtained from D. Littman (Skirball Institute of Biomolecular Medicine, New York, New York), were provided by D. Kioussis and N. Harker (National Institute for Medical Research, London, United Kingdom). All experiments were approved by the University of York Animal Procedures and Ethics Committee and performed under UK Home Office license. *L. donovani* (LV9) was maintained by passage in *Rag2*$^{-/-}$ mice. Mice were infected by injecting 3×10^7 amastigotes i.v. via the lateral tail vein. Sm (35 mg/kg; Sequoia Research Products Ltd.) was administered daily via oral gavage for 7 days. Vehicle-treated mice received citrate-buffered saline, pH 3.5. For combined therapy, Sm- or vehicle-treated animals received a single dose of Sb^v (Pentostam, a gift from V. Yardley, London School of Hygiene and Tropical Medicine, United Kingdom), at the doses indicated in Results, or saline as a control. At the indicated times, mice were killed, spleens removed, and parasite burdens determined from Giemsa-stained impression smears. Parasite burden was expressed as Leishman-Donovan units (LDU; the number of parasites per 1,000 host cell nuclei × organ weight; ref. 22).

In vitro antigen stimulation. BMDCs were generated from mouse bone marrow progenitors in DMEM supplemented with 10% fetal calf serum and 10% GM-CSF, and infected with *L. donovani* amastigotes at a multiplicity of infection of 10:1. Whole spleen cell suspensions were isolated from control or drug-treated *L. donovani*–infected mice and cultured at 37°C in the presence of infected BMDCs for 3 hours followed by incubation with brefeldin-A for 4 hours. Cells were then stained for CD3 in combination with CD4 and/or CD8 and analyzed for intracellular cytokine production.

Flow cytometry. Cells were surface stained with PE-Cy7–conjugated anti-CD3, PerCP-conjugated anti-CD4, APC Cy7–conjugated anti-CD8, Alexa Fluor 647–conjugated F4/80, or PE-conjugated anti-CD11b (BD Biosciences — Pharmingen). LIVE/DEAD fixable aqua dead cell stain kit (Invitrogen) was added in some experiments. Cells were then fixed with 2% paraformaldehyde, permeabilized with 0.5% saponin, and stained with Pacific blue–conjugated anti–IFN-γ, PE-conjugated anti–TNF-α, APC-conjugated anti–IL-10, and FITC-conjugated IL-17a (eBioscience). B cell frequency was assessed by staining spleen cell suspensions with PerCP-conjugated anti-CD45R (BD Biosciences — Pharmingen). LTi cells were identified as described previously (28). FITC-conjugated anti-CD45, Pacific blue–conjugated anti-CD3, Alexa Fluor 647–conjugated-anti CD11c, Pacific blue–conjugated anti-CD45R, and PE-conjugated anti–IL-7Rα were all purchased from eBioscience, and PerCP-conjugated anti-CD4 was purchased from BD Biosciences — Pharmingen. Cells were analyzed using a cyAn flow cytometer and analyzed using Summit software (Beckman Coulter).

Confocal microscopy. Frozen spleen sections (6–40 μm) were acetone fixed and labeled with a biotinylated anti-CD31 (PECAM-1; eBioscience) or purified rat anti-mouse pan–endothelial cell antigen antibody (Meca32; BD Biosciences — Pharmingen) and detected with Alexa Fluor 488 streptavidin conjugate or with a fluorochrome-conjugated goat anti-rat antibody (both from Invitrogen). Polyclonal rabbit anti-mouse Ki67 antibody detected with an Alexa Fluor 647–conjugated goat anti-rabbit (Abcam) and/or a Cy3-labeled monoclonal antibody against α-SMA (clone 1A4; Sigma-Aldrich) were used in combination with anti-CD31 to identify proliferating endothelial cells and recruitment of perivascular mesenchymal cells, respectively. To assess microarchitecture, sections were stained with mAbs to MMM (MOMA-1; Acris Antibodies), MZM (ERTR9; Bachem), T cell zone FRC (Alexa Fluor 488–conjugated podoplanin; gp38; eBioscience), FDC (FDCMI), Pacific blue–conjugated CD3, FITC-conjugated B220, Alexa Fluor 647–conjugated F4/80, and MAdCAM-1 biotin conjugated (Serotec). Fluorochrome-conjugated goat anti-rat antibodies were used for detection of purified antibodies and streptavidin conjugated secondary for the detection of biotin-conjugated antibodies. Sections were counterstained with DAPI and mounted in Pro-long Gold anti-fade (Invitrogen) and visualized using a Carl Zeiss inverted LSM META 510 confocal microscope. Quantification of CD31- and Meca32-labeled vessels, $gp38^+$ FRCs and FDCs was performed on in at least 9 randomly selected fields per mouse and at least 10 mice per time point. The degree of staining was detected using Adobe Photoshop CS3, and the fraction of positively stained pixels relative to the whole number of pixels was expressed as percentage of area positive for CD31 or Meca32.

Whole mount staining. Whole mount staining was performed as described previously (81). Briefly, spleens were fixed in 4% PFA at 4°C for 2–3 hours and washed in PBS plus 0.15% Triton-X100. 100-μm sections were made using a Vibratome (Leica Microsystems). Sections were washed and blocked in 5% goat serum and subsequently stained with a Cy3-labeled monoclonal antibody against α-SMA. Whole mounts were dehydrated serially in 25%, 50%, 75%, and 100% methanol and then optically cleared using Benzyl Alcohol and Benzyl Benzoate (BABB; Sigma-Aldrich) before imaging. Background autofluorescence was collected by excitation with 488 nm laser and emission collected between 490 nm and 515 nm. Confocal images acquired on a Zeiss Meta510NLO are presented as a 3-dimensional rendering of serial sections generated using Volocity software (Improvision).

Microangiography. Fluorescent microangiography was conducted on naive and infected C57BL/6 mice. Animals were injected via the tail vein with FITC-dextran (500,000 MW; Sigma-Aldrich). Spleens were removed and examined using a Zeiss Stereolumar V12 fluorescence stereomicroscope.

Generation of bone marrow chimeras. B6.CD45.1 recipient mice were lethally irradiated using a split dose regimen or 2× 550 rads given 24 hours apart and delivered using a RS2000 X-ray irradiator (RadSource Inc.). After the second dose, recipients were injected intravenously with 1×10^7 B6.*Rorc*$^{-/-}$ (RORγ-deficient mice; CD45.2) or wild-type B6 (CD45.2) bone marrow cells. Mice were provided with Baytril-treated water for 3 weeks after irradiation and were used for experiments 8–12 weeks after bone marrow reconstitution.

Determination of NO production by macrophages. 2×10^6 splenocytes from infected mice were incubated in a 24-well plate (Corning) for 1 hour at 37°C in RPMI and 10% FCS. Nonadherent cells were removed by extensive washing in RPMI (20°C). Adherent cells were then cultured for 24 hours at 37°C in RPMI supplemented with 10% FCS. Supernatants were harvested at 24 hours and assayed for NO levels using a Griess Regent System according to the manufacturer's instructions (Promega).

Real-time RT-PCR. RNA was isolated from whole spleens using an RNeasy kit according to the manufacturer's instructions (Qiagen). RNA was then reverse transcribed into cDNA using the first-strand cDNA synthesis kit according to the manufacturer's instructions (Invitrogen). Oligonucleotides used for the specific amplification were *Il10* and *Hprt* (22); *Tnf* forward, 5′-CATCTTCTCAAAATTCGAGTGA-3′; *Tnf* reverse, 5′-TGGGAGTAGACAAGGTACAAC-3′; *Il17a* forward, 5′-GCTCCAGAAGGCCCTCAG-3′; *Il17a* reverse, 5′-CTTTCCCTCCGCATTGACA-3′. Real-time quantitative RT-PCR was performed with the SYBR green PCR kit in an ABI Prism

7000 sequence detection system (Applied Biosystems) according to the manufacturer's instructions. Expression of target genes was normalized to HPRT and expressed as relative expression using the change in cycle threshold (ΔΔCT) analysis method (relative expression of the gene in Sm treated compared to its vehicle control counterpart).

Statistics. Data are expressed as mean ± SEM. Comparison of multiple groups was performed by 1-way ANOVA followed by Dunn's or Tukey post-test as appropriate. When 2 groups were compared, comparison was performed using the 2-tailed unpaired Student's *t* test (for data following a Gaussian distribution) and the Mann-Whitney test (for data that did not assume Gaussian distribution). D'Agostino and Pearson omnibus normality test was used to test for Gaussian distribution. A probability of less than 5% ($P < 0.05$) was considered to be statistically significant. All statistical analyses were performed with Prism software (version 5.01; GraphPad Inc.). ED_{50} values were calculated using nonlinear transform fit using Prism software (version 5.01; GraphPad Inc.).

Acknowledgments

This work was funded by grants from the British Medial Research Council and the Wellcome Trust. The authors thank the staff of the Department of Biology Technology Facility and Biological Services Facility for their expert assistance, Dimitris Kioussis and Nicky Harker for providing *Rorc*$^{-/-}$ mice, and Charles Lacey for comments on the manuscript.

Received for publication September 29, 2009, and accepted in revised form January 20, 2010.

Address correspondence to: Paul M. Kaye, Centre for Immunology and Infection, Hull York Medical School and Department of Biology, University of York, Wentworth Way, York YO10 5YW, United Kingdom. Phone: 44.1904.328840; Fax: 44.1904.328844; E-mail: pmk2@york.ac.uk.

1. Buysschaert I, Carmeliet P, Dewerchin M. Clinical and fundamental aspects of angiogenesis and anti-angiogenesis. *Acta Clin Belg*. 2007;62(3):162–169.
2. Carmeliet P. Manipulating angiogenesis in medicine. *J Intern Med*. 2004;255(5):538–561.
3. Tugues S, et al. Antiangiogenic treatment with sunitinib ameliorates inflammatory infiltrate, fibrosis, and portal pressure in cirrhotic rats. *Hepatology*. 2007;46(6):1919–1926.
4. Batchelor TT, et al. AZD2171, a pan-VEGF receptor tyrosine kinase inhibitor, normalizes tumor vasculature and alleviates edema in glioblastoma patients. *Cancer Cell*. 2007;11(1):83–95.
5. Luttun A, et al. Revascularization of ischemic tissues by PlGF treatment, and inhibition of tumor angiogenesis, arthritis and atherosclerosis by anti-Flt1. *Nat Med*. 2002;8(8):831–840.
6. Mendel DB, et al. In vivo antitumor activity of SU11248, a novel tyrosine kinase inhibitor targeting vascular endothelial growth factor and platelet-derived growth factor receptors: determination of a pharmacokinetic/pharmacodynamic relationship. *Clin Cancer Res*. 2003;9(1):327–337.
7. Alvar J, Yactayo S, Bern C. Leishmaniasis and poverty. *Trends Parasitol*. 2006;22(12):552–557.
8. Chappuis F, et al. Visceral leishmaniasis: what are the needs for diagnosis, treatment and control? *Nat Rev Microbiol*. 2007;5(11):873–882.
9. Ghalib H, Modabber F. Consultation meeting on the development of therapeutic vaccines for post kala azar dermal leishmaniasis. *Kinetoplastid Biol Dis*. 2007;6:7.
10. Alvar J, Croft S, Olliaro P. Chemotherapy in the treatment and control of leishmaniasis. *Adv Parasitol*. 2006;61:223–274.
11. Murray HW, Delph-Etienne S. Roles of endogenous gamma interferon and macrophage microbicidal mechanisms in host response to chemotherapy in experimental visceral leishmaniasis. *Infect Immun*. 2000;68(1):288–293.
12. Badaro R, et al. Immunotherapy for drug-refractory mucosal leishmaniasis. *J Infect Dis*. 2006; 194(8):1151–1159.
13. Murphy ML, Cotterell SE, Gorak PM, Engwerda CR, Kaye PM. Blockade of CTLA-4 enhances host resistance to the intracellular pathogen, Leishmania donovani. *J Immunol*. 1998;161(8):4153–4160.
14. Murray HW. Interleukin 10 receptor blockade--pentavalent antimony treatment in experimental visceral leishmaniasis. *Acta Trop*. 2005;93(3):295–301.
15. Murray HW, Lu CM, Brooks EB, Fichtl RE, DeVecchio JL, Heinzel FP. Modulation of T-cell costimulation as immunotherapy or immunochemotherapy in experimental visceral leishmaniasis. *Infect Immun*. 2003;71(11):6453–6462.
16. Zubairi S, Sanos SL, Hill S, Kaye PM. Immunotherapy with OX40L-Fc or anti-CTLA-4 enhances local tissue responses and killing of Leishmania donovani. *Eur J Immunol*. 2004;34(5):1433–1440.
17. Kaye PM, et al. The immunopathology of experimental visceral leishmaniasis. *Immunol Rev*. 2004; 201:239–253.
18. Engwerda CR, Kaye PM. Organ-specific immune responses associated with infectious disease. *Immunol Today*. 2000;21(2):73–78.
19. Engwerda CR, et al. A role for tumor necrosis factor-alpha in remodelling the splenic marginal zone during Leishmania donovani infection. *Am J Pathol*. 2002; 161(2):429–437.
20. Stanley AC, Engwerda CR. Balancing immunity and pathology in visceral leishmaniasis. *Immunol Cell Biol*. 2007;85(2):138–147.
21. Smelt SC, Engwerda CR, McCrossen M, Kaye PM. Destruction of follicular dendritic cells during chronic visceral leishmaniasis. *J Immunol*. 1997; 158(8):3813–3821.
22. Ato M, Stager S, Engwerda CR, Kaye PM. Defective CCR7 expression on dendritic cells contributes to the development of visceral leishmaniasis. *Nat Immunol*. 2002;3(12):1185–1191.
23. Beattie L, Engwerda CR, Wykes M, Good MF. CD8+ T lymphocyte-mediated loss of marginal metallophilic macrophages following infection with Plasmodium chabaudi chabaudi AS. *J Immunol*. 2006; 177(4):2518–2526.
24. Cadman ET, et al. Alterations of splenic architecture in malaria are induced independently of Toll-like receptors 2, 4, and 9 or MyD88 and may affect antibody affinity. *Infect Immun*. 2008;76(9):3924–3931.
25. Radwanska M, Guirnalda P, De Trez C, Ryffel B, Black S, Magez S. Trypanosomiasis-induced B cell apoptosis results in loss of protective anti-parasite antibody responses and abolishment of vaccine-induced memory responses. *PLoS Pathog*. 2008;4(5):e1000078.
26. Benedict CA, De Trez C, Schneider K, Ha S, Patterson G, Ware CF. Specific remodelling of splenic architecture by cytomegalovirus. *PLoS Pathog*. 2006; 2(3):e16.
27. Mueller SN, et al. Viral targeting of fibroblastic reticular cells contributes to immunosuppression and persistence during chronic infection. *Proc Natl Acad Sci U S A*. 2007;104(39):15430–15435.
28. Scandella E, et al. Restoration of lymphoid organ integrity through the interaction of lymphoid tissue-inducer cells with stroma of the T cell zone. *Nat Immunol*. 2008;9(6):667–675.
29. Zijlstra EE, el-Hassan AM. Leishmaniasis in Sudan. Visceral leishmaniasis. *Trans R Soc Trop Med Hyg*. 2001;95(Suppl 1):S27–S58.
30. Bajenoff M, Glaichenhaus N, Germain RN. Fibroblastic reticular cells guide T lymphocyte entry into and migration within the splenic T cell zone. *J Immunol*. 2008;181(6):3947–3954.
31. Junt T, Scandella E, Ludewig B. Form follows function: lymphoid tissue microarchitecture in antimicrobial immune defence. *Nat Rev Immunol*. 2008; 8(10):764–775.
32. Kosco-Vilbois MH. Introduction: FDC in health and disease. *Semin Immunol*. 2002;14(4):249.
33. Mebius RE, Kraal G. Structure and function of the spleen. *Nat Rev Immunol*. 2005;5(8):606–616.
34. Alexandre-Pires G, Pais D, Correia M, Pina JA. Leishmaniosis--a report about the microvascular and cellular architecture of the infected spleen in Canis familiaris. *Microsc Res Tech*. 2006;69(4):227–235.
35. Lokmic Z, Lammermann T, Sixt M, Cardell S, Hallmann R, Sorokin L. The extracellular matrix of the spleen as a potential organizer of immune cell compartments. *Semin Immunol*. 2008;20(1):4–13.
36. Hipp MM, et al. Sorafenib, but not sunitinib, affects function of dendritic cells and induction of primary immune responses. *Blood*. 2008;111(12):5610–5620.
37. van Cruijsen H, et al. Sunitinib-induced myeloid lineage redistribution in renal cell cancer patients: CD1c+ dendritic cell frequency predicts progression-free survival. *Clin Cancer Res*. 2008;14(18):5884–5892.
38. Zwick S, et al. Assessment of vascular remodelling under antiangiogenic therapy using DCE-MRI and vessel size imaging. *J Magn Reson Imaging*. 2009; 29(5):1125–1133.
39. Murray HW, et al. Acquired resistance and granuloma formation in experimental visceral leishmaniasis. Differential T cell and lymphokine roles in initial versus established immunity. *J Immunol*. 1992; 148(6):1858–1863.
40. van Rooijen N, Kors N, Kraal G. Macrophage subset repopulation in the spleen: differential kinetics after liposome-mediated elimination. *J Leukoc Biol*. 1989;45(2):97–104.
41. Eberl G, Marmon S, Sunshine MJ, Rennert PD, Choi Y, Littman DR. An essential function for the nuclear receptor RORgamma(t) in the generation of fetal lymphoid tissue inducer cells. *Nat Immunol*. 2004; 5(1):64–73.
42. Engwerda CR, Murphy ML, Cotterell SE, Smelt SC, Kaye PM. Neutralization of IL-12 demonstrates the existence of discrete organ-specific phases in the control of Leishmania donovani. *Eur J Immunol*. 1998; 28(2):669–680.
43. Pitta MG, et al. IL-17 and IL-22 are associated with protection against human kala azar caused by Leishmania donovani. *J Clin Invest*. 2009; 119(8):2379–2387.
44. Alexander J, Carter KC, Al-Fasi N, Satoskar A, Brombacher F. Endogenous IL-4 is necessary for effective drug therapy against visceral leishmaniasis. *Eur J Immunol*. 2000;30(10):2935–2943.
45. Murray HW. Interferon-gamma, the activated mac-

rophage, and host defense against microbial challenge. *Ann Intern Med.* 1988;108(4):595–608.
46. Squires KE, et al. Immunochemotherapy for visceral leishmaniasis: a controlled pilot trial of antimony versus antimony plus interferon-gamma. *Am J Trop Med Hyg.* 1993;48(5):666–669.
47. Sundar S, Rosenkaimer F, Murray HW. Successful treatment of refractory visceral leishmaniasis in India using antimony plus interferon-gamma. *J Infect Dis.* 1994;170(3):659–662.
48. Stager S, Maroof A, Zubairi S, Sanos SL, Kopf M, Kaye PM. Distinct roles for IL-6 and IL-12p40 in mediating protection against Leishmania donovani and the expansion of IL-10+ CD4+ T cells. *Eur J Immunol.* 2006;36(7):1764–1771.
49. Veress B, Omer A, Satir AA, El Hassan AM. Morphology of the spleen and lymph nodes in fatal visceral leishmaniasis. *Immunology.* 1977;33(5):605–610.
50. Keenan CM, Hendricks LD, Lightner L, Johnson AJ. Visceral leishmaniasis in the German shepherd dog. II. Pathology. *Vet Pathol.* 1984;21(1):80–86.
51. Bajenoff M, et al. Stromal cell networks regulate lymphocyte entry, migration, and territoriality in lymph nodes. *Immunity.* 2006;25(6):989–1001.
52. Sher A, Pearce E, Kaye P. Shaping the immune response to parasites: role of dendritic cells. *Curr Opin Immunol.* 2003;15(4):421–429.
53. Fiorentino DF, et al. IL-10 acts on the antigen-presenting cell to inhibit cytokine production by Th1 cells. *J Immunol.* 1991;146(10):3444–3451.
54. Kane MM, Mosser DM. The role of IL-10 in promoting disease progression in leishmaniasis. *J Immunol.* 2001;166(2):1141–1147.
55. Kim SJ, et al. Circulating monocytes expressing CD31: implications for acute and chronic angiogenesis. *Am J Pathol.* 2009;174(5):1972–1980.
56. Kubota Y, et al. M-CSF inhibition selectively targets pathological angiogenesis and lymphangiogenesis. *J Exp Med.* 2009;206(5):1089–1102.
57. Pollard JW. Trophic macrophages in development and disease. *Nat Rev Immunol.* 2009;9(4):259–270.
58. Sunderkotter C, Goebeler M, Schulze-Osthoff K, Bhardwaj R, Sorg C. Macrophage-derived angiogenesis factors. *Pharmacol Ther.* 1991;51(2):195–216.
59. Carmeliet P. Angiogenesis in health and disease. *Nat Med.* 2003;9(6):653–660.
60. Koch AE. The role of angiogenesis in rheumatoid arthritis: recent developments. *Ann Rheum Dis.* 2000; 59(Suppl 1):i65–i71.
61. Bagli E, Xagorari A, Papetropoulos A, Murphy C, Fotsis T. Angiogenesis in inflammation. *Autoimmun Rev.* 2004;3(Suppl 1):S26.
62. Majno G. Chronic inflammation: links with angiogenesis and wound healing. *Am J Pathol.* 1998; 153(4):1035–1039.
63. Szekanecz Z, Gaspar L, Koch AE. Angiogenesis in rheumatoid arthritis. *Front Biosci.* 2005;10:1739–1753.
64. Lane P, et al. Lymphoid tissue inducer cells in adaptive CD4 T cell dependent responses. *Semin Immunol.* 2008;20(3):159–163.
65. Veiga-Fernandes H, et al. Tyrosine kinase receptor RET is a key regulator of Peyer's patch organogenesis. *Nature.* 2007;446(7135):547–551.
66. Carragher DM, Rangel-Moreno J, Randall TD. Ectopic lymphoid tissues and local immunity. *Semin Immunol.* 2008;20(1):26–42.
67. Rangel-Moreno J, et al. Omental milky spots develop in the absence of lymphoid tissue-inducer cells and support B and T cell responses to peritoneal antigens. *Immunity.* 2009;30(5):731–743.
68. Sundar S, Murray HW. Cure of antimony-unresponsive Indian visceral leishmaniasis with amphotericin B lipid complex. *J Infect Dis.* 1996;173(3):762–765.
69. Sundar S, et al. Amphotericin B treatment for Indian visceral leishmaniasis: response to 15 daily versus alternate-day infusions. *Clin Infect Dis.* 2007; 45(5):556–561.
70. Bhattacharya SK, et al. Phase 4 trial of miltefosine for the treatment of Indian visceral leishmaniasis. *J Infect Dis.* 2007;196(4):591–598.
71. Sundar S, et al. New treatment approach in Indian visceral leishmaniasis: single-dose liposomal amphotericin B followed by short-course oral miltefosine. *Clin Infect Dis.* 2008;47(8):1000–1006.
72. Molina I, et al. Efficacy of liposomal amphotericin B for secondary prophylaxis of visceral leishmaniasis in HIV-infected patients. *J Antimicrob Chemother.* 2007;60(4):837–842.
73. Troya J, Casquero A, Refoyo E, Fernandez-Guerrero ML, Gorgolas M. Long term failure of miltefosine in the treatment of refractory visceral leishmaniasis in AIDS patients. *Scand J Infect Dis.* 2008;40(1):78–80.
74. Dietze R, et al. Phase 2 trial of WR6026, an orally administered 8-aminoquinoline, in the treatment of visceral leishmaniasis caused by Leishmania chagasi. *Am J Trop Med Hyg.* 2001;65(6):685–689.
75. Gasser RAJ, Magill AJ, Oster CN, Franke ED, Grögl M, Berman JD. Pancreatitis induced by pentavalent antimonial agents during treatment of leishmaniasis. *Clin Infect Dis.* 1994;18(1):83–90.
76. Hepburn NC, Siddique I, Howie AF, Beckett GJ, Hayes PC. Hepatotoxicity of sodium stibogluconate in leishmaniasis. *Lancet.* 1993;342:238–239.
77. Sundar S, Agrawal N, Arora R, Agarwal D, Rai M, Chakravarty J. Short-course paromomycin treatment of visceral leishmaniasis in India:14-day vs 21-day treatment. *Clin Infect Dis.* 2009;49(6):914–918.
78. Das VN, et al. Magnitude of unresponsiveness to sodium stibogluconate in the treatment of visceral leishmaniasis in Bihar. *Natl Med J India.* 2005; 18(3):131–133.
79. Apetoh L, Tesniere A, Ghiringhelli F, Kroemer G, Zitvogel L. Molecular interactions between dying tumor cells and the innate immune system determine the efficacy of conventional anticancer therapies. *Cancer Res.* 2008;68(11):4026–4030.
80. Van Geertruyden JP, et al. HIV-1 immune suppression and antimalarial treatment outcome in Zambian adults with uncomplicated malaria. *J Infect Dis.* 2006;194(7):917–925.
81. Foster K, et al. Contribution of neural crest-derived cells in the embryonic and adult thymus. *J Immunol.* 2008;180(5):3183–3189.